ACS OMEGA

http://pubs.acs.org/journal/acsodf

Article

Study on the Assembly Structure Variation of Cetyltrimethylammonium Bromide on the Surface of Gold Nanoparticles

Runmei Li, Zhuorui Wang, Xuefan Gu, Cong Chen, Yaya Zhang, and Daodao Hu*

Cite This: *ACS Omega* 2020, 5, 4943−4952

Read Online

ACCESS | Metrics & More | Article Recommendations

ABSTRACT: In this work, the self-assembly behavior of cetyltrimethylammonium bromide (CTAB) on the surface of citrate-capped gold nanoparticles (AuNPs) in solution has been studied by UV−vis absorption spectroscopy, fluorescence probe techniques, ζ potentiometric methods, transmission electron microscopy, etc. The UV−vis spectra show that the color with the increase of CTAB for the mixture containing CTAB and a given amount of AuNPs changes from red to blue and then to red. The absolute value of ζ potential corresponding to this color change decreases initially and then increases. Specially, the reversible color change, from red to blue and then to red, could be observed only in the case of a gradual addition of a AuNP solution to a CTAB solution; however, this reversible change is not suitable for the mixture formed in a reverse order of mixing. The results from pyrene used as the fluorescence probe indicate that the features in the fluorescence spectrum (including fluorescence quenching, I_1/I_3, and the excimer) well correspond to those from the UV−vis spectrum mentioned above. Based on the experimental results, the mechanism of the assembly structure variation of CTAB on the surface of negatively charged AuNPs was proposed. For a given amount of AuNPs, the assembly structure of CTAB on the surface of AuNPs undergoes the transformation from a monolayer to a bilayer with the increase of CTAB. In the case of the concentration of CTAB far beyond its critical micelle concentration (CMC) and the higher ratio of CTAB and AuNPs, there is a possibility of the formation of an extra micellar structure only after the formation of a double-layer structure.

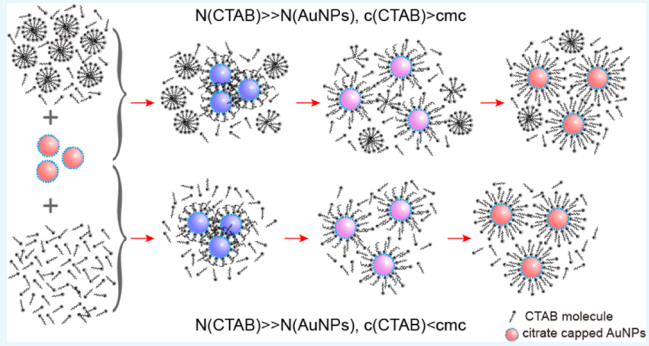

INTRODUCTION

Surfactants play a key role in the synthesis and functionalization of metal nanoparticles.[1] Generally, a surfactant seems to be one of the desirable structure-directing agents inducing anisotropic growth in aqueous media through binding to specific nanocrystal facets, achieving the controlled growth and shape of the particles.[2] By binding to some crystal surfaces and decreasing the surface energy, they also act as a stabilizer against coagulation.[3] In addition, the presence of these moieties on the surface of nanoparticles causes new and/or improved properties, which makes them important in biological activity, catalytic behavior, chemical sensing,[4−12] optical properties, etc.[3] Hence, deepening the understanding of the interaction between surfactants and metal nanoparticles is of significance for their application.

Among the surfactants used in the preparation of metallic nanoparticles, cetyltrimethylammonium bromide (CTAB) has been the most typical representative to grow gold nanoparticles (AuNPs) with different morphologies, such as gold nanorods (AuNRs),[13−15] hexagonal and triangular nanocrystalline gold plates,[16] bimetallic nanoparticles,[17] high-index faceted gold nanocrystals,[18,19] and gold nanocubes.[20]

The development of the methods for preparing metal nanomaterials with various morphologies has promoted the exploration of the growth mechanism as well as the surface structure of the NPs capped with surfactants. In the synthesis of rod-shaped gold nanoparticles, Nikoobakht and El-Sayed proposed that CTAB as the major and cosurfactant tetradodecylammonium bromide (TOAB) as the minor component in the mixture form a bilayer structure, rather than a micelle, around AuNRs.[21] This conclusion was also supported by Murphy and Mann et al. They reported that a surfactant micelle is not involved in controlling the shape anisotropy of metallic nanoparticles.[22] Since then, the model of

Received: November 11, 2019
Accepted: January 30, 2020
Published: March 4, 2020

https://dx.doi.org/10.1021/acsomega.9b03823
ACS Omega 2020, 5, 4943−4952

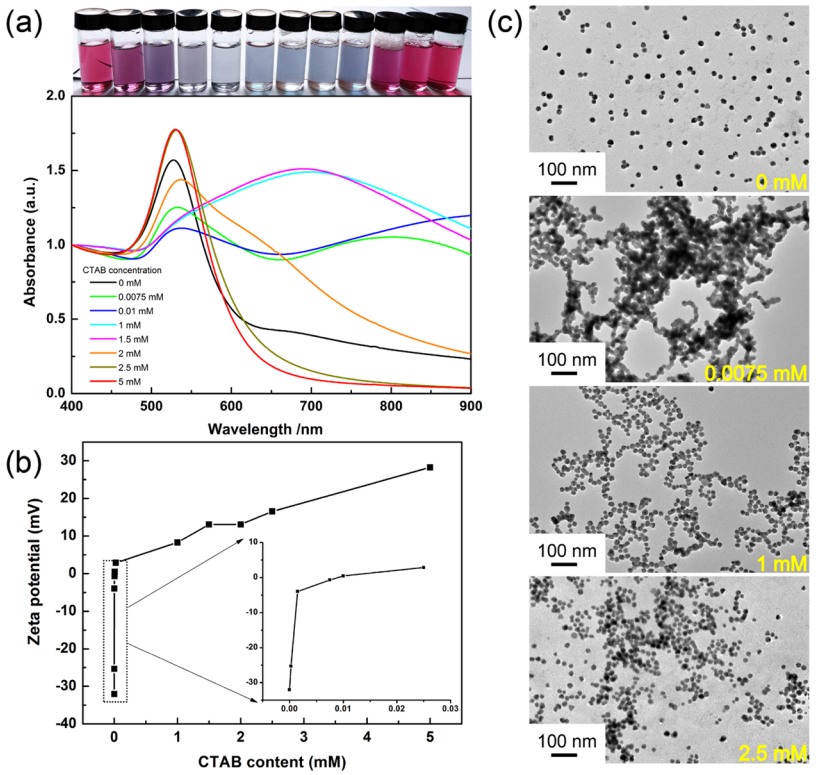

Figure 1. (a) Change in the UV−vis spectrum with different CTAB concentrations for the mixture of CTAB and a given amount of AuNPs (1.50×10^{12} NPs/mL), and photos (top) of the corresponding samples. (b) Change in the ζ potential of citrate-capped AuNPs (1.50×10^{12} NPs/mL) with different concentrations of CTAB. (c) Transmission electron microscopy (TEM) images of AuNPs in the presence of different CTAB contents.

a CTAB bilayer structure rather than a micelle around the surface of AuNPs has been widely approved.[23−25] This bilayer structure was also proved in the preparation of AuNPs using CTAB and cetyltrimethylammonium chloride (CTAC) as a cosurfactant.[26] Murphy et al. using 1-naphthol as a probe also proved the rationality of the double-layer structure of CTAB on the surface of gold nanorods,[27] and they also verified this structure on the surface of AuNPs by replacing CTAB with the polymerizable surfactant 11-(acryloyloxy)-undecyl-trimethyl ammonium bromide in the preparation of polymer-stabilized AuNPs.[28] Baruah et al. found that the stability of the double-layer structure of CTAB formed on AuNPs could be enhanced by nonylamine (NA) as a cosurfactant.[29] Recently, the double-layer structure of CTAB on the surface of AuNPs was confirmed by a multiscale model that combines first-principles methods with atomistic and mesoscopic simulations.[30]

Although the double-layer structure of CTAB formed in the preparation of AuNRs has almost become a consensus, even now, the assembly structure of CTAB on the surface of already-prepared negatively charged AuNPs is still controversial. Recently, on the basis of the results of small-angle neutron scattering (SANS), small-angle X-ray scattering (SAXS) techniques, etc., Skoglund et al. proposed that the negatively charged AgNPs were stabilized by CTAB cluster micelles rather than a double-layer structure of CTAB.[31] Based on the color change of the negatively charged AuNPs induced by CTAB or CTAC at their concentrations exceeding the critical micelle concentration (CMC), a similar conclusion was also drawn.[32,33] Although the CTAB bilayer structure is easier to form on the facets of gold nanorods than on spherical gold nanoparticles,[2] it is also possible to produce the bilayer structure of CTAB on the surface of negatively charged AuNPs.

We believe that the difference in the reported assembly structure of CTAB on the negatively charged AuNPs is related to the relative proportion of CTAB and AuNPs in the experimental process. As the positively charged CTAB molecules are added into the solution containing a given amount of the negatively charged AuNPs, the assembly structure of CTAB onto the surface of AuNPs and their stability change with CTAB. With the increase in the amount of CTAB added, the assembly structure of CTAB onto the surface of AuNPs undergoes a change from an incomplete to a complete hydrophobic single layer.[34] During the above process, not only the charge on AuNPs gradually decreases but also the surface hydrophobicity enhances. As a result, the tendency of AuNPs aggregation is gradually enhanced. It is worth noting that the aggregation of AuNPs leads to the irreversible fusion among AuNPs if the amount of CTAB covered on AuNPs is not sufficient to block the contact among AuNPs.[35] However, the aggregation of AuNPs covered with monolayer CTAB is reversible due to enough isolation of the CTAB layer. In this case, the hydrophobic tail of the added CTAB can insert into the CTAB single layer on the surface of AuNPs through a hydrophobic interaction gradually to form a complete bilayer structure of CTAB, similar to a lipid bilayer.[28] The above transformation from the monolayer to the bilayer makes the aggregated AuNPs disperse due to the enhancement of electrostatic repulsion and hydrophilicity. During this transformation, if the formation of a CTAB monolayer on AuNPs is reasonable, it is difficult to understand that CTAB molecules bound in the monolayer can be completely released

https://dx.doi.org/10.1021/acsomega.9b03823
ACS Omega 2020, 5, 4943−4952

to participate in the formation of CTAB micelles together with the added CTAB.

Obviously, the assembly structure of CTAB on the surface of AuNPs is closely related to the relative proportion of CTAB and AuNPs rather than the concentration of CTAB. It was reported in the literature that AuNPs have a stable dispersion state when the concentration of CTAB approaches CMC. Based on this finding, it was concluded that AuNPs were stabilized by surrounding CTAB micelles, which may be a coincidence. In fact, for a given surfactant, its CMC is different from that in the presence of an electrolyte. The presence of the negatively charged AuNPs may decrease the CMC of the surfactant, which is similar to that of electrolyte.[36] Therefore, only when the concentration of CTAB far exceeds its CMC, both the CTAB double-layer structure and micelles around AuNPs could be simultaneously present. Actually, this situation has been described in the literature.[37,38]

To explore the influence of exogenous CTAB on the aggregation of the prepared negatively charged AuNPs as well as the corresponding mechanism, this work detailedly studied the behaviors for a series of specially designed mixtures containing CTAB and citrate-capped AuNPs using UV−vis spectroscopy, transmission electron microscopy, ζ potential analysis, and fluorescence probe techniques. The following main findings are included in our investigations: (1) CTAB micelles are not stable in AuPN solution and are prone to disassemble and reassemble on the surface of AuNPs. (2) As long as CTAB/AuNPs are in a proper ratio, the above-mentioned assembly could occur regardless of the CTAB concentration being lower or higher than its CMC. (3) The mixing sequence of the positively charged CTAB and the negatively charged AuNPs can directly impact the reversibility of the aggregation of AuNPs induced by the CTAB assembly. These results could be explained in terms of the change in the self-assembly structure of CTAB from a single layer to a double layer and the ζ potential of the corresponding assemblies. The present investigation is expected to not only help understand the self-assembled structure of CTAB on the surface of AuNPs but also provide a basis for the research associated with the special effects of surfactants on the surface of AuNPs and their applications, for example, based on the sensitivity in electrostatic interaction, developing some approaches to monitor negatively charged species (surfactants, polyelectrolytes, biomolecules, etc.) and methods to prepare some arrays using AuNPs loaded with the monolayer or bilayer of CTAB as a structural unit.

RESULTS AND DISCUSSION

Effect of CTAB on the UV−Vis Spectrum of AuNPs. Figure 1a depicts the UV−vis absorption spectra of the mixture (mixture A) containing different concentrations of CTAB and 1.50×10^{12} NPs/mL of AuNPs. Photos of the corresponding typical color change of the mixtures are shown on the top of Figure 1a. Overall, the trend of the color change in AuNPs with the increase of CTAB is similar to the results reported in the literature.[32] This phenomenon, the color variation from red to blue and then from blue to red for the AuNP solution with the increase of CTAB, could be explained in terms of the change in the charge feature of AuNPs. Due to gradual adsorption of CTAB with a positive charge onto the surface of AuNPs with a negative charge, the original negative charge of AuNPs gradually increases to zero and then from zero to a positive charge. This change directly results in the change of the dispersity of AuNPs.

From the precise spectral variation (Figure 1a) related to the above-mentioned phenomenon, the as-prepared citrate-capped AuNPs have a typical surface plasmon resonance (SPR) peak at 526 nm (black curve), and this plasmon absorption slightly red-shifts to 530 nm after CTAB is introduced from 0.0075 to 0.01 mM. This slight red shift is attributed to the partial replacement of citrate on the surface of AuNPs by CTAB molecules.[39,40] At the same time, an additional broad peak centered at 600−900 nm appears with different intensities, corresponding to a purple-to-blue color change for AuNPs. This phenomenon suggests the aggregation of AuNPs in different degrees.[40] Interestingly, the broad peak evidently blue-shifts as CTAB concentration is increased to above 1 mM and even almost disappears when CTAB concentration is further increased above 2 mM, whereas the SPR peak at 530 nm increases steadily in intensity (orange curve). As CTAB concentration is increased to 5 mM (red curve), the absorption in the range of 600−900 nm completely disappears, and the SPR peak located at 530 nm turns out to be almost the same as that of a pure AuNP solution (526 nm).

The evolution feature of the above UV−vis spectra unambiguously indicates that the aggregation of AuNPs also occurs even when the concentration of CTAB exceeds its CMC, implying that the dispersed AuNPs in the presence of CTAB is not stabilized by the structure of CTAB micelles. As we proposed above, in the higher concentration of CTAB as shown in Figure 1, the stability of AuNP dispersion is achieved by a CTAB double-layer structure rather than CTAB micelles.[31] In our opinion, the evolution of CTAB assembly structures on AuNPs could be explained by the following corresponding changes in ζ potential, as shown in Figure 1b.

It can be seen that the ζ potential for AuNPs is −36 mV in the absence of CTAB, which is relevant to that of a citrate anion absorbed on the surface of AuNPs, resulting in a dispersed state with a red color due to electrostatic repulsion.[41] For AuNP solutions in the presence of CTAB ranging from 0 to 0.025 mM, the ζ potential of the mixtures remarkably increases from −36 mV to nearly 0 mV and corresponds to the dramatic aggregation of AuNPs in blue or gray color. Then, the ζ potential increases from 0 mV to a positive value when the CTAB concentration is greater than 0.025 mM and finally reaches +28.26 mV as the CTAB concentration reaches 5 mM. In this situation, the AuNP solution presents a gradual change in color from blue to red, which implies the increase in the stability of AuNPs. This trend is coincident with that in the reported literature[23,32,42] and is in good agreement with the change in the spectral results (Figure 1a). Significantly, the ζ potential curve shown in Figure 1b presents three linear trends, −32.04 to −3.96 mV, −3.96 to +2.876 mV, and 2.876 to +28.26 mV, which correspond to the CTAB concentration ranging from 0 to 0.0015 mM, 0.0015 to 0.025 mM, and 0.025 to 5 mM, respectively, implying that the three stages are related to the structural transformation of CTAB assembled on the surface of AuNPs.

In the first stage, the ζ potential increases from the negative to nearly zero in the concentration of CTAB ranging from 0 to 0.0015 mM. This change corresponds to the formation of an incomplete single layer of CTAB, and the corresponding driving force is attributed to the electrostatic interaction between the positively charged ammonium moiety of CTAB and the negatively charged AuNPs. Since CTAB molecules

https://dx.doi.org/10.1021/acsomega.9b03823
ACS Omega 2020, 5, 4943−4952

with a positive charge adsorb onto the bare negatively charged AuNPs, the increase of the ζ potential with increasing CTAB is relatively fast. In the second stage, the ζ potential slowly changes to around zero in the concentration of CTAB ranging from 0.0015 to 0.025 mM, corresponding to the transition from an incomplete monolayer to a complete single layer driven by the electrostatic interaction. Due to the decrease in the negative charge and increase in the steric resistance, CTAB molecules adsorbed onto AuNPs inhibit the subsequent CTAB molecules from being adsorbed onto AuNPs. Therefore, in this stage, the corresponding ζ potential shows a relatively slow increase with the increase of CTAB. In the last stage, the ζ potential increases from nearly zero to positive in the concentration of CTAB ranging from 0.025 to 5 mM, and this stage involves the formation of a perfect bilayer of CTAB and the ensuing formation of CTAB micelles. Obviously, the driving force in this stage is ascribed to the hydrophobic interaction involving the insertion of free hydrophobic tails of CTAB into the hydrophobic palisade already formed on the AuNPs. In this stage, the insertion of the hydrophobic alkyl chain of CTAB into the hydrophobic palisade is relatively difficult and the increase of the ζ potential with the increase of CTAB is relatively slow.

To verify the difference in the dispersed state of AuNPs in the presence of a typical concentration of CTAB, we recorded TEM images for the AuNP samples in the presence of a typical concentration of CTAB (0, 0.0075, 1.0, and 2.5 mM) [see UV−vis spectra (Figure 1a)], and the results are shown in Figure 1c. Clearly, these images present the process from dispersion to aggregation and to re-dispersion. These results well match with the corresponding changes in the UV−vis spectra and ζ potentials. According to the evolution of CTAB assembling structures onto AuNPs with the increase of CTAB, the resultant structures correspond to without CTAB, an incomplete monolayer, an incomplete bilayer, and a complete bilayer.

Additionally, the slight red shift of the SPR peak for the mixture of AuNPs and CTAB compared with that for AuNPs indicates that there is a strong interaction between CTAB and AuNPs. Thus, CTAB molecules adsorbed on the surface of AuNPs do not have a significant desorption and together with newly added CTAB are involved in the formation of the micelles. Certainly, the above observation does not mean that it is impossible to form CTAB micelles in the mixture of CTAB and AuNPs. In fact, there is still enough CTAB in the mixture after the amount of CTAB satisfies the formation of bilayers on the surface of AuNPs, and the formation of CTAB micelles in the mixture is possible. A similar situation could be found in the literature.[37,38] On the basis of above-mentioned discussion, we think that the conclusion in the reported literature regarding the formation of CTAB micelles rather than the CTAB bilayer around AuNPs is probably related to the less amount of AuNPs used in the experiments, and this conclusion is an experimental coincidence rather than a necessity.

According to our proposal, in the mixture of AuNPs and CTAB, the lower the concentration of AuNPs, the lower the CTAB concentration inducing the color change of AuNPs. Namely, the color change of the mixtures of AuNPs and CTAB from red to blue and then to red is possible in the case of the CTAB concentration below its CMC as long as the number of CTAB molecules is far more than that of AuNPs. For our hypothesis to be confirmed, 20 μL of AuNP solution, instead of 2 mL of AuNPs used in the experiments shown in Figure 1, was introduced into 2 mL of CTAB solutions with different concentrations less than CMC, and the UV−vis absorption spectra of the corresponding mixtures were detected, as shown in Figure 2.

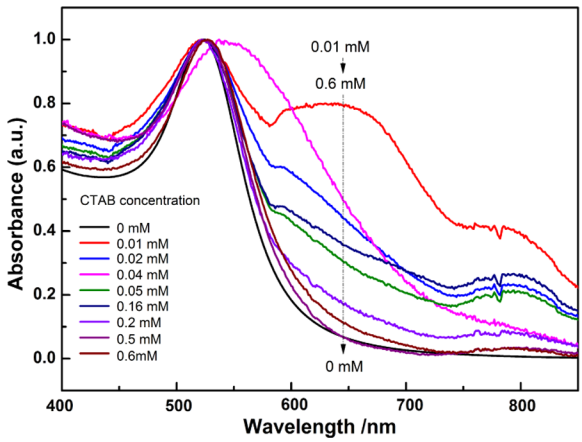

Figure 2. Change in the UV−vis spectra with different concentrations of CTAB (<CMC) for the mixture of CTAB and a given amount of AuNPs (3×10^{10} NPs/mL).

As expected, when the CTAB concentration is in the range of 0.01−0.16 mM, compared with AuNP solution, the SPR peak at 526 nm hardly shifts, while an obvious new peak appears in the range of 600−800 nm, implying in this case that the AuNPs are aggregated even with a CTAB concentration of 0.01 mM. With the increase of the CTAB concentration from 0.01 to 0.6 mM, the intensity of the absorption at the wavelength above 600 nm continuously decreases until the spectrum becomes similar to that of AuNPs. The above results clearly show that the conversion from the aggregated into the dissociated AuNPs still occurs even with a CTAB concentration far lower than CMC. Apparently, this process is unlikely to involve the formation of CTAB micelles. In this case, the only possible structure for AuNPs stabilized by CTAB is the bilayer rather than the micelle.

As a summary of the experimental results shown in Figures 1 and 2, Figure 3 gives a schematic model of the self-assembly structure variation of CTAB on the surface of citrate-capped AuNPs. This model involves six typical states, according to the amount of CTAB adsorbed onto the surface of AuNPs. These are state 1 (citrate-capped AuNPs), state 2 (an incomplete monolayer of CTAB), state 3 (a complete monolayer of CTAB), state 4 (an imperfect bilayer of CTAB), state 5 (a perfect bilayer of CTAB), and state 6 (the coexistence of the bilayer and micelle of CTAB). Among them, state 1−state 2, state 2−state 3, and state 3−state 6 correspond to the first, the second, and the last stage in the ζ potential, respectively. The corresponding color in turn changes from red to purple, blue, purple, and red. The above process could be explained in terms of the self-assembly of the positively charged CTAB onto the negatively charged AuNPs and in turn resulting in the change of the ζ potential. It is particularly pointed out here that the above change depends not only on the CTAB concentration but also on the ratio of CTAB and AuNP. Additionally, only after the formation of the bilayer of CTAB on the surface of AuNPs, the CTAB micelles around AuNPs could form when the amount of CTAB was enough to form the micelles. To

https://dx.doi.org/10.1021/acsomega.9b03823
ACS Omega 2020, 5, 4943−4952

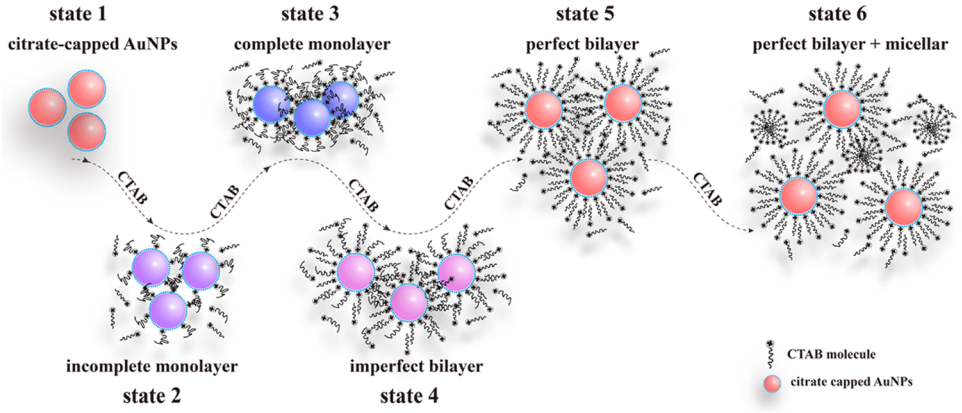

Figure 3. Proposed possible mechanism for the variation in the assembly structure of CTAB on the citrate-capped AuNPs.

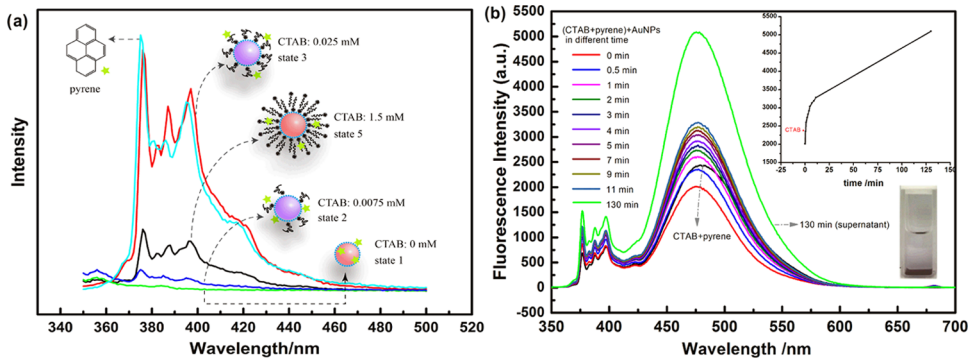

Figure 4. (a) Fluorescence spectra of pyrene (1.629×10^{-8} M) in a series of mixtures with different ratios of AuNPs to CTAB as given in the mixture C (AuNPs: 1.50×10^{12} NPs/mL). (b) Change in the pyrene (0.036 mM) fluorescence spectrum and intensity (inset) with time for the mixture containing CTAB and AuNPs. CTAB: 1 mM, AuNPs: 1.50×10^{12} NPs/mL.

verify the proposed model, we carried out the following experiments.

Pyrene Probing of the Assembly Structure of CTAB on the AuNPs. Figure 4a shows the fluorescence spectra of pyrene in a series of mixtures with different ratios of AuNPs to CTAB as given in the mixture C. A characteristic emission peak of pyrene in pure water (cyan curve) is observed, while the fluorescence is almost completely quenched in the presence of AuNPs (green curve, state 1). This phenomenon can be explained using the energy transfer mechanism of the high-efficiency quenching effect of AuNPs on fluorescence probes.[43] Note that here quenching belongs to a dynamic fluorescence quenching, which depends only on collision, since there is no special chemical interaction between pyrene and AuNPs. As a result, compared with bare AuNPs with an exposed surface, which can easily contact with the probe, AuNP solution in the presence of CTAB should show a weaker fluorescence quenching due to AuNPs covered by CTAB in varying degrees. As expected, compared with that for state 1 (green curve), the fluorescence quenching for the AuNP solution containing 0.0075 mM CTAB (blue curve, state 2) shows a certain degree of inhibition. With the increase in the CTAB concentration to 0.025 mM (red curve, state 3), the fluorescence quenching is more significantly decreased, accompanying a noticeable decrease in I_1/I_3, indicating that pyrene obviously locates not only far from AuNPs but also in a hydrophobic environment.[44] Evidently, the existence of CTAB micelles in this situation (0.025 mM $\ll$ CMC) is impossible and thus the only available hydrophobic domain for the location of pyrene is at least not the micelles of CTAB. We believe that this hydrophobic microenvironment was formed here by the compact structure of hydrophobic tails of CTAB molecules adsorbed on the surface of AuNPs. Generally, the long alkyl chain of CTAB facing toward the aqueous phase is likely in a compact structure,[45] making the hydrophobic layer formed by CTAB alkyl chains dense. In this case, pyrene finds it difficult to enter the interior of the hydrophobic layer and perches only on the boundary. Consequently, the probability for pyrene to directly contact the surface of AuNPs is reduced, strongly decreasing the quenching effect of AuNPs. However, compared with that of state 3, the fluorescence quenching of pyrene is visibly enhanced again as the concentration of CTAB reaches 1.5 mM (black curve, corresponding to state 5), but I_1/I_3 hardly changes. In this situation, if there were CTAB micelles in the mixture, pyrene would be gathered into the inner core of the micelles and the chance of collision between AuNPs and pyrene would be further reduced, which would cause the fluorescence intensity for state 5 (black curve) to be higher than that for state 3 (red curve). Obviously, the above result could not be explained in terms of micelles. We believe that pyrene located in the double layer of CTAB is more likely to fit well with the fluorescence spectrum of state 5. In the CTAB interdigitated palisade layer, pyrene is not only in a hydrophobic domain but also has a greater movability due to CTAB with the long alkyl chain and the big head adsorbed on the surface of AuNPs,[46] allowing pyrene to approach AuNPs. As a result, the fluorescence of pyrene in the case of state 5 is more strongly quenched compared with that in state 3. After

https://dx.doi.org/10.1021/acsomega.9b03823
ACS Omega 2020, 5, 4943−4952

all, however, the movability of pyrene in the palisade layer has a certain limitation; thus, the quenching effect is relatively mild compared with that in state 1.

For the evidence regarding the conversion of CTAB micelles into the self-assembled bilayer of CTAB on the surface of AuNPs to be acquired, the mixture D, that is, 1 mL of AuNP solution added into 1 mL of CTAB solution (2 mM) containing pyrene (0.036 mM), was obtained, and the change in the fluorescence spectrum of the mixture with time is shown in Figure 4. In the mixture, CTAB concentration exceeds CMC (~0.9 mM), which makes pyrene concentrate into the micelle of CTAB. As expected, in the results shown in Figure 4b, a particularly obvious excimer emission peak centered at 475 nm[47] can be observed in the CTAB solution (black curve). Expectedly, the emission intensity of the excimer dramatically decreases once AuNPs are added, which might be largely related to the dilution induced by the addition of AuNPs. Surprisingly, the emission of the excimer for the CTAB−AuNP mixture increases progressively with time until 130 min. At this time, the blue-black precipitate deposits at the bottom of the cuvette, and the supernatant has a stronger excimer emission (green curve) than CTAB without AuNPs. Obviously, the above phenomenon implies that the pyrene content located in the local microdomain constantly increases after CTAB micelles are mixed with AuNPs. In other words, the CTAB micelles in AuNPs are unstable.

It is worth mentioning that the deposited AuNPs mentioned above did not turn into a stable suspension even by either forced shaking or ultrasonic treatment, indicating that a large amount of CTAB in the supernatant fails to be assembled on the surface of deposited AuNPs to disperse AuNPs. We suspected that this might be related to the strong interaction between the high concentration of hydrophobic pyrene and the hydrophobic palisade layer in CTAB micelles,[46] preventing further disintegration of CTAB micelles for the self-assembly onto the surface of AuNPs. For this conjecture to be confirmed, the CTAB solutions (1 and 2 mM) without pyrene were separately added into the above-mentioned aggregated AuNPs, and the UV−vis absorption spectra of the corresponding mixtures were recorded. The expected results are shown in Figure 5. For the supernatant, there is no peak in the UV−vis absorption spectrum (blue curve). However, when 1 or 2 mM of the CTAB solution without pyrene was added into aggregated AuNP solution, the blue-black precipitated AuNPs immediately returned to a red stable solution and the obvious peaks at 530 nm (gray curve and purple curve) appeared, which are similar to the SPR peak of AuNPs.[48] These results reveal that the aforementioned aggregated AuNPs can be dispersed by the addition of a CTAB solution.

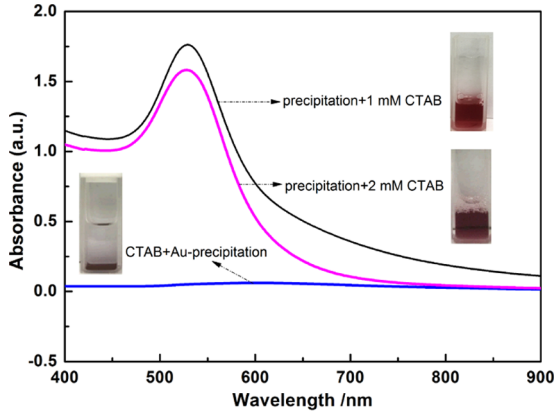

Figure 5. UV−vis spectra of the supernatant of aggregated AuNPs induced by CTAB and the aggregates suspended in different concentrations of CTAB. The aggregated AuNPs obtained from the experiment in Figure 4b.

On the basis of the above experimental results, the mechanism of the effect of the interaction between CTAB micelles and AuNPs on the fluorescence behavior of pyrene discussed in Figure 4b was proposed. As shown in Figure 6, by adding the negatively charged AuNP solution to the CTAB micelle solution, the positively charged headgroups of CTAB micelles tend to bind to the surface of AuNPs, causing the gradual disintegration of CTAB micelles and releasing pyrene from the core of CTAB micelles continuously. Then, the released pyrene is enriched in the core of free CTAB micelles in the mixture, enhancing the emission of the excimer due to the increase in the local pyrene concentration. This process does not stop until the hydrophobic CTAB monolayer is formed on the surface of AuNPs due to the strong interaction between the high concentration of hydrophobic pyrene and the hydrophobic palisade layer in CTAB micelles in the supernatant, preventing further disintegration of CTAB micelles. Simultaneously, the assembly of CTAB on the AuNPs not only reduces the absolute value of the ζ potential of AuNPs but also enhances their hydrophobicity, which leads to the aggregation of AuNPs. Addition of CTAB solution into the aggregates of AuNPs loaded with CTAB monolayer can makes the aggregates redisperse due to formation of mutually repulsive AuNPs loaded with CTAB bilayer. This mechanism further verifies that the negatively charged AuNPs could be stabilized through a CTAB bilayer rather than CTAB micelles.

Effect of the Mixing Order of CTAB and AuNPs on the Aggregation Behavior of AuNPs. Seemingly, the mixing sequence of a CTAB solution and a AuNP solution should not affect the final aggregation behavior of AuNPs. However, this is not the case. When 1 mL of a CTAB (2 mM) aqueous solution was dropwise added into 1 mL of a AuNP solution (3×10^{12} NPs/mL), the mixture immediately changed from red to purple and then to blue and finally a gray precipitate was formed (process A in Figure 7). However, when the two solutions were mixed in the opposite order, the mixture first turned from red to purple and then to a blue color and finally, after standing for a long time, a blue precipitate was formed (process B in Figure 7). More interestingly, the gray precipitate generated in process A failed to re-disperse through the further addition of a CTAB solution and, in contrast, on the further addition of a CTAB solution into the blue precipitate formed in process B, the mixture turned to a transparent red solution.

In fact, the above phenomena could be explained in terms of the mechanism presented in Figure 3. In the case of the dropwise addition of a CTAB solution into a AuNP solution, the interaction between CTAB micelles and AuNPs makes micelles disassemble. For process A in Figure 7, at the beginning, because very few CTAB micelles are surrounded by too many AuNPs, there is not enough CTAB to form a protective layer on the surface of AuNPs for decreasing AuNP aggregation, which is easy to lead to an irreversible coalescence of red AuNPs to form blue and even gray aggregates. It has been documented that as AuNPs approach to distances less than ~0.5 nm, an increasing electron tunneling current neutralizes the charge separation at the junction between the spheres and an attractive Coulombic force can be generated

https://dx.doi.org/10.1021/acsomega.9b03823
ACS Omega 2020, 5, 4943−4952

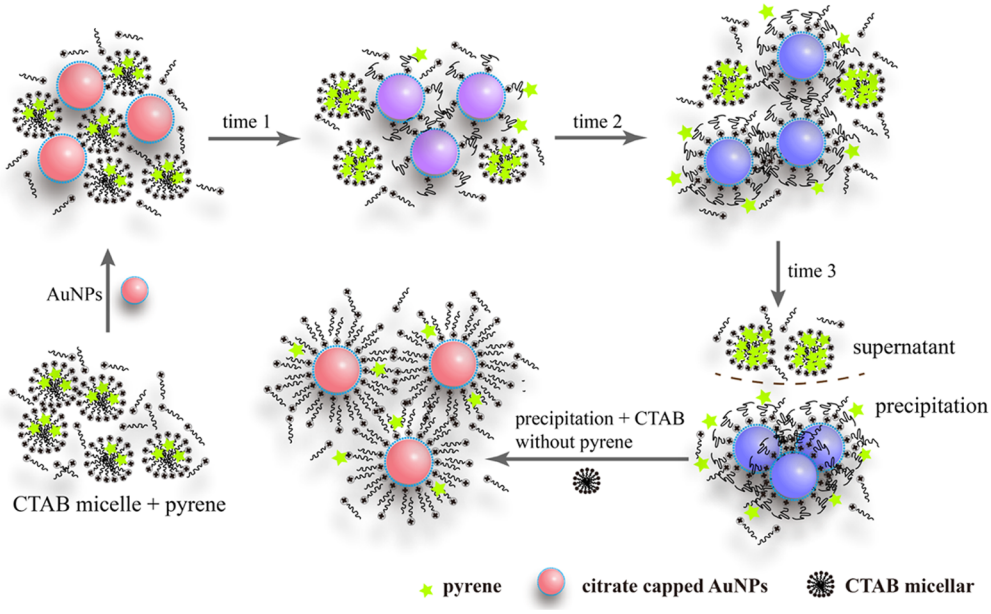

Figure 6. Proposed mechanism for the effect of the interaction between CTAB micelles and AuNPs on the microenvironment of the fluorescence probe pyrene.

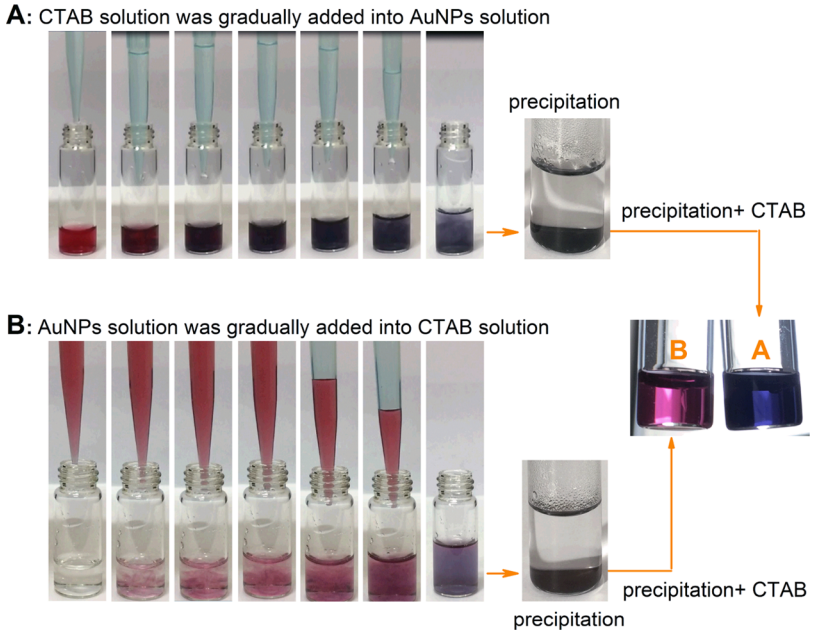

Figure 7. Photos showing the color change in the solutions formed by (A) CTAB and (B) AuNPs in different mixing orders and their corresponding resulted precipitates dispersed in CTAB solutions.

between them to enable full dimer particle convergence to a single, larger nanoparticle.[35] Figure 8A indicates the coalescent AuNPs from the gray precipitate. Clearly, it is impossible to disperse these coalescent AuNPs through the addition of extra CTAB. However, in the case of the dropwise addition of a AuNP solution into a CTAB solution (process B in Figure 7), very few AuNPs are surrounded by too many CTAB micelles at first and the amount of CTAB is enough to form a perfect bilayer onto the surface of AuNPs. The resulting CTAB bilayer ensures the stability of AuNPs. As the amount of AuNPs added into the mixture increases, the CTAB bilayer formed on the AuNPs is gradually destroyed to transfer to the surface of the newly added AuNPs until leading to the formation of the

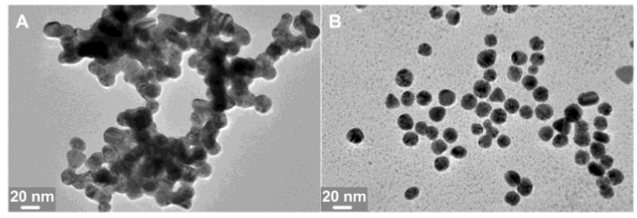

Figure 8. TEM images of the precipitations from the mixtures made in different mixing orders. (A) Addition of CTAB into AuNPs and (B) addition of AuNPs into CTAB.

monolayer of CTAB on the surface of each AuNP in the mixture. At this point, the CTAB monolayer causes a decrease

https://dx.doi.org/10.1021/acsomega.9b03823
ACS Omega 2020, 5, 4943−4952

in the electrostatic repulsion and an increase in the surface hydrophobicity of AuNPs, finally resulting in the blue aggregates of AuNPs (Figure 8B). Fortunately, the coalescence between adjacent AuNPs is hindered due to the coverage of the CTAB monolayer on the surface of AuNPs in this case, and the CTAB monolayer on the surface of AuNPs can be converted into the CTAB bilayer by the further addition of CTAB molecules (Figure 7B). Indeed, the irreversible and reversible aggregations here are similar to the "aggregate" of AuNPs irreversibly bound together by primary chemical or metallurgical bonds and the "agglomerate" of AuNPs weakly and reversibly bound by van der Waals or similar secondary bonds, respectively.[49] Apparently, from another aspect, the above experiments support the variation model for the assembly of CTAB from forming monolayer to bilayer structures on the surface of the negatively charged AuNPs with the increase of CTAB.

CONCLUSIONS

In view of the inconsistency regarding the assembly structure of CTAB on the surface of the negatively charged AuNPs reported in the literature, the self-assembly structure variation of CTAB on the surface of AuNPs with the increase of CTAB was systematically investigated. On the basis of our research results, the following conclusions could be drawn: (1) For a mixture containing CTAB and a given amount of AuNPs, with the increase of the CTAB concentration, the color of the mixture changes from red to blue and then to red. This process corresponds to a gradual formation of the CTAB monolayer and the bilayer on AuNPs, accompanying the change in the ζ potential of AuNPs from negative to zero and then to positive. (2) The self-assembly structure of CTAB on the surface of AuNPs relies on the relative proportion of CTAB and AuNPs. The formation of the CTAB bilayer on the surface of AuNPs has the advantages over that of CTAB micelles. When enough amount of CTAB exists in the AuNP solution, only after the formation of the bilayer of CTAB on the surface of AuNPs could the CTAB micelles form around AuNPs. (3) The mixing sequence of a CTAB solution and a AuNP solution strongly affects the reversibility of the aggregates formed by CTAB and AuNPs. The aggregates formed by the gradual addition of AuNPs into a CTAB solution can be re-dispersed through the further addition of CTAB, whereas the aggregated AuNPs induced by the dropwise addition of a CTAB solution into a AuNP solution are difficult to be re-dispersed.

These findings not only contribute to deepen the understanding of the interaction between CTAB and AuNPs but also have valuable references in applications based on the assembly of CTAB and AuNPs. Additionally, the fluorescence probe used in this investigation also provides new insight into the exploration of the interaction between CTAB and AuNPs.

EXPERIMENTAL SECTION

Materials. Tetrachloroauric acid ($HAuCl_4{\cdot}4H_2O$, purity ≥99.9%), chlorhydric acid (HCl, AR), and dichloromethane (AR) were purchased from Sinopharm Chemical Reagent Co., Ltd. (Shanghai, China). Cetyltrimethylammonium bromide (CTAB) and trisodium citrate (AR) were received from TIANLI Chemical Reagents Ltd. (Tianjin, China). Pyrene was obtained from Aldrich. All reactants were used without further purification. Milli-Q water was used in all of the experiments. All used glassware was treated with aqua regia, rinsed in Milli-Q water, and oven-dried prior to use.

Synthesis of Gold Nanoparticles. The citrate-stabilized AuNPs were prepared via previously reported methods.[50] Briefly, 1 mL of aqueous $HAuCl_4$ (25 mM) was injected into 150 mL of a boiling sodium citrate solution (2.2 mM), and the solution was kept boiling for 10 min. This led to a series of color changes from purple to blue, bluish gray, and red, indicating the formation of citrate-capped AuNPs used as the seed solution (~10 nm, ~3×10^{12} NPs/mL). Then, the solution was cooled down to 90 °C and 2 mL of the obtained solution was taken out. The final step was the addition of 1 mL of the $HAuCl_4$ solution (25 mM) to the remaining seed solution and keeping the temperature of the solution constant at a temperature of 90 °C for 30 min. After the final step was repeated once again, the reaction was quenched in an ice-water bath. This process produced AuNPs with a size of ~20 nm. The concentration of the as-prepared AuNPs was approximately the same as that of the seed particles (~3×10^{12} NPs/mL).

Experimental Processes for the Determination of UV−Vis Spectra and ζ Potential and for TEM. *Preparation of a Mixture of AuNPs and CTAB with a Concentration Exceeding CMC.* A CTAB solution (2 mL, 0−10 mM) was well mixed with 2 mL of AuNPs (~3×10^{12} NPs/mL), which resulted in a series of AuNPs/CTAB solutions (mixture A).

Preparation of a Mixture of AuNPs and CTAB with a Concentration below CMC. By introducing 20 μL of AuNPs (~3×10^{12} NPs/mL) into 2 mL of an aqueous CTAB solution (0−0.6 mM), the desired AuNPs/CTAB mixtures were obtained (mixture B).

UV−visible spectra of mixtures A and B were recorded with a Lambda 35 UV−vis spectrometer (PerkinElmer, Waltham). Transmission electron microscopy (TEM) images were recorded on a JEM-2100 instrument (JEOL, Tokyo, Japan) with an accelerating voltage of 200 kV (20 μL of the sample was dropped onto a carbon-coated Cu grid and dried in air). Effective surface charges on the surface of AuNPs (1.5×10^{12} NPs/mL) in the presence of different contents of CTAB (0, 0.00025, 0.0075, 0.01, 0.025, 1.0, 1.5, 2, 2.5, 5, and 10 mM) were measured using a ζ potential analyzer (Malvern Instruments Zetasizer, Worcestershire, U.K.). Each sample was measured three times to obtain an average value. It should be noted that all of the solutions mentioned above for determination were analyzed immediately after mixing because of their unstable characteristics.

Recording Dynamic Color Changes of the AuNPs/CTAB System. A total of 1 mL of 2 mM CTAB was dropwise added into a cuvette containing 1 mL of a AuNP solution (~3×10^{12} NPs/mL), and typical color changes at different time intervals were immediately pictured. Then, this operation was repeated after reversing the mixing sequence.

Preparation of Mixtures for Recording Fluorescence Spectra. Fluorescence spectra were recorded using an F-7000 fluorescence spectrometer (Shimadzu, Japan) (excitation wavelength: 340 nm; slit width: 2.5/2.5 nm; voltage: 700 V).

Preparation of the Mixtures Containing a Lower Concentration of Pyrene. CTAB (2 mL) with different concentrations was well mixed with 2 mL of AuNPs (~3×10^{12} NPs/mL) to obtain a series of mixtures (the final concentrations of CTAB: 0, 0.0075, 0.025, and 1.5 mM). Then, 100 μL of a saturated aqueous solution of pyrene was

https://dx.doi.org/10.1021/acsomega.9b03823
ACS Omega 2020, 5, 4943−4952

separately added into the above solutions (the final concentration of pyrene was 1.629×10^{-8} M) (mixture C), and the mixtures were immediately monitored by fluorescence spectroscopy with the excitation wavelength of 340 nm.

Preparation of the Mixtures Containing a Higher Concentration of Pyrene. A total of 200 μL of a 0.54 mM pyrene solution (using dichloromethane as the solvent) was taken into a 10 mL beaker, and then, the beaker was slowly rotated to form a liquid membrane on its inner wall until the complete evaporation of dichloromethane. To the beaker coated with pyrene, 3 mL of 2 mM CTAB was added, and then, the beaker was placed in an ultrasonic bath to be treated for 30 min. The above CTAB solution (1 mL) containing the pyrene probe (0.036 mM) was mixed with 1 mL of AuNPs ($\sim 3 \times 10^{12}$ NPs/mL), and the change in the fluorescence spectrum with time was immediately recorded with the excitation wavelength of 340 nm. Aggregation accompanying sedimentation took place in the mixture during fluorescence determination. In this situation, the fluorescence spectra of the supernatant and suspension were recorded (mixture D).

AUTHOR INFORMATION

Corresponding Author

Daodao Hu − *Engineering Research Center of Historical and Cultural Heritage Protection, Ministry of Education, School of Materials Science and Engineering, Shaanxi Normal University, Xi'an 710062, China;* orcid.org/0000-0001-5226-2086; Email: daodaohu@snnu.edu.cn

Authors

Runmei Li − *Engineering Research Center of Historical and Cultural Heritage Protection, Ministry of Education, School of Materials Science and Engineering, Shaanxi Normal University, Xi'an 710062, China*

Zhuorui Wang − *Engineering Research Center of Historical and Cultural Heritage Protection, Ministry of Education, School of Materials Science and Engineering, Shaanxi Normal University, Xi'an 710062, China*

Xuefan Gu − *College of Chemistry and Chemical Engineering, Xi'an Shiyou University, Xi'an 710065, China*

Cong Chen − *Engineering Research Center of Historical and Cultural Heritage Protection, Ministry of Education, School of Materials Science and Engineering, Shaanxi Normal University, Xi'an 710062, China*

Yaya Zhang − *Engineering Research Center of Historical and Cultural Heritage Protection, Ministry of Education, School of Materials Science and Engineering, Shaanxi Normal University, Xi'an 710062, China*

Complete contact information is available at: https://pubs.acs.org/10.1021/acsomega.9b03823

Author Contributions

D.H. and X.G. contributed to the conception of the study; R.L. drafted the manuscript and conducted overall experiments; R.L. and D.H. performed the data analyses; and Z.W., C.C., and Y.Z. revised the manuscript.

Funding

This study was supported by the National Natural Science Foundation of China (Grant No. 21505103).

Notes

The authors declare no competing financial interest.

REFERENCES

(1) Wang, Z. L.; Mohamed, M. B.; Link, S.; El-Sayed, M. A. Crystallographic Facets and Shapes of Gold Nanorods of Different Aspect Ratios. *Surf. Sci.* **1999**, *440*, L809−L814.

(2) Nikoobakht, B.; El-Sayed, M. A. Preparation and Growth Mechanism of Gold Nanorods (NRs) Using Seed-Mediated Growth Method. *Chem. Mater.* **2003**, *15*, 1957−1962.

(3) Nikoobakht, B.; El-Sayed, M. A. Evidence for Bilayer Assembly of Cationic Surfactants on the Surface of Gold Nanorods. *Langmuir* **2001**, *17*, 6368−6374.

(4) Zhao, C.; Hong, C.; Lin, Z.; Chen, X.; Huang, Z. Detection of Malachite Green using a colorimetric aptasensor based on the inhibition of the peroxidase-like activity of gold nanoparticles by cetyltrimethylammonium ions. *Microchim. Acta* **2019**, *186*, No. 322.

(5) Zhang, Z.; Wang, H.; Chen, Z.; Wang, X.; Choo, J.; Chen, L. Plasmonic colorimetric sensors based on etching and growth of noble metal nanoparticles: Strategies and applications. *Biosens. Bioelectron.* **2018**, *114*, 52−65.

(6) Nguyen, L. T. N.; Park, C. Y.; Park, J. P.; Kailasa, S. K.; Park, T. J. Synergistic molecular assembly of an aptamer and surfactant on gold nanoparticles for the colorimetric detection of trace levels of As^{3+} ions in real samples. *New J. Chem.* **2018**, *42*, 11530−11538.

(7) Sun, X.; Liu, R.; Liu, Q.; Fei, Q.; Feng, G.; Shan, H.; Huan, Y. Colorimetric sensing of mercury (II) ion based on anti-aggregation of gold nanoparticles in the presence of hexadecyl trimethyl ammoniumbromide. *Sens. Actuators, B* **2018**, *260*, 998−1003.

(8) Wang, Y.; Wang, Y.; Wang, W.; Sun, K.; Chen, L. Reporter-Embedded SERS Tags from Gold Nanorod Seeds: Selective Immobilization of Reporter Molecules at the Tip of Nanorods. *ACS Appl. Mater. Interfaces* **2016**, *8*, 28105−28115.

(9) Chen, L.; Li, J.; Chen, L. Colorimetric Detection of Mercury Species Based on Functionalized Gold Nanoparticles. *ACS Appl. Mater. Interfaces* **2014**, *6*, 15897−15904.

(10) Chen, L.; Fu, X.; Lu, W.; Chen, L. Highly Sensitive and Selective Colorimetric Sensing of Hg^{2+} Based on the Morphology Transition of Silver Nanoprisms. *ACS Appl. Mater. Interfaces* **2013**, *5*, 284−290.

(11) Fu, X.; Lou, T.; Chen, Z.; Lin, M.; Feng, W.; Chen, L. "Turn-on" Fluorescence Detection of Lead Ions Based on Accelerated Leaching of Gold Nanoparticles on the Surface of Graphene. *ACS Appl. Mater. Interfaces* **2012**, *4*, 1080−1086.

(12) Lou, T.; Chen, Z.; Wang, Y.; Chen, L. Blue-to-Red Colorimetric Sensing Strategy for Hg^{2+} and Ag^{+} via Redox-Regulated Surface Chemistry of Gold Nanoparticles. *ACS Appl. Mater. Interfaces* **2011**, *3*, 1568−1573.

(13) Gole, A.; Murphy, C. J. Seed-Mediated Synthesis of Gold Nanorods: Role of the Size and Nature of the Seed. *Chem. Mater.* **2004**, *16*, 3633−3640.

(14) Liang, Y.; Xie, Y.; Chen, D.; Guo, C.; Hou, S.; Wen, T.; Yang, F.; Deng, K.; Wu, X.; Smalyukh, I. I.; Liu, Q. Symmetry Control of Nanorod Superlattice Driven by a Governing Force. *Nat. Commun.* **2017**, *8*, No. 1410.

(15) Peng, R.; Si, Y.; Deng, T.; Zheng, J.; Li, J.; Yang, R.; Tan, W. A Novel SERS Nanoprobe for the Ratiometric Imaging of Hydrogen Peroxide in Living Cells. *Chem. Commun.* **2016**, *52*, 8553−8556.

(16) Chu, H.-C.; Kuo, C.-H.; Huang, M. H. Thermal Aqueous Solution Approach for the Synthesis of Triangular and Hexagonal Gold Nanoplates with Three Different Size Ranges. *Inorg. Chem.* **2006**, *45*, 808−813.

(17) Baruah, B.; Kiambuthi, M. Facile Synthesis of Silver and Bimetallic Silver−Gold Nanoparticles and Their Applications in Surface Enhanced Raman Scattering. *RSC Adv.* **2014**, *4*, 64860−64870.

(18) Ming, T.; Feng, W.; Tang, Q.; Wang, F.; Sun, L.; Wang, J.; Yan, C. Growth of Tetrahexahedral Gold Nanocrystals with High-Index Facets. *J. Am. Chem. Soc.* **2009**, *131*, 16350−16351.

(19) Zhang, J.; Langille, M. R.; Personick, M. L.; Zhang, K.; Li, S.; Mirkin, C. A. Concave Cubic Gold Nanocrystals with High-Index Facets. *J. Am. Chem. Soc.* **2010**, *132*, 14012−14014.

(20) Sisco, P. N.; Murphy, C. J. Surface-Coverage Dependence of Surface-Enhanced Raman Scattering from Gold Nanocubes on Self-Assembled Monolayers of Analyte. *J. Phys. Chem. A* **2009**, *113*, 3973−3978.
(21) Nikoobakht, B.; El-Sayed, M. A. Evidence for Bilayer Assembly of Cationic Surfactants on the Surface of Gold Nanorods. *Langmuir* **2001**, *17*, 6368−6374.
(22) Johnson, C. J.; Dujardin, E.; Davis, S. A.; Murphy, C. J.; Mann, S. Growth and Form of Gold Nanorods Prepared by Seed-mediated, Surfactant-directed Synthesis. *J. Mater. Chem.* **2002**, *12*, 1765−1770.
(23) Sau, T. K.; Murphy, C. J. Self-Assembly Patterns Formed upon Solvent Evaporation of Aqueous Cetyltrimethylammonium Bromide-Coated Gold Nanoparticles of Various Shapes. *Langmuir* **2005**, *21*, 2923−2929.
(24) Gao, J.; Bender, C. M.; Murphy, C. J. Dependence of the Gold Nanorod Aspect Ratio on the Nature of the Directing Surfactant in Aqueous Solution. *Langmuir* **2003**, *19*, 9065−9070.
(25) Tiwari, N. R.; Rathore, A.; Prabhune, A.; Kulkarni, S. K. Gold Nanoparticles for Colorimetric Detection of Hydrolysis of Antibiotics by Penicillin G Acylase. *Adv. Biosci. Biotechnol.* **2010**, *01*, 322−329.
(26) Dewi, M. R.; Laufersky, G.; Nann, T. A highly efficient ligand exchange reaction on gold nanoparticles: preserving their size, shape and colloidal stability. *RSC Adv.* **2014**, *4*, 34217−34220.
(27) Alkilany, A. M.; Frey, R. L.; Ferry, J. L.; Murphy, C. J. Gold Nanorods as Nanoadmicelles: 1-Naphthol Partitioning into a Nanorod-Bound Surfactant Bilayer. *Langmuir* **2008**, *24*, 10235−10239.
(28) Alkilany, A. M.; Murphy, C. J. Gold Nanoparticles with a Polymerizable Surfactant Bilayer: Synthesis, Polymerization, and Stability Evaluation. *Langmuir* **2009**, *25*, 13874−13879.
(29) Baruah, B.; Craighead, C.; Abolarin, C. One-Phase Synthesis of Surface Modified Gold Nanoparticles and Generation of SERS Substrate by Seed Growth Method. *Langmuir* **2012**, *28*, 15168−15176.
(30) Gao, H.-M.; Liu, H.; Qian, H.-J.; Jiao, G.-S.; Lu, Z.-Y. Multiscale Simulations of Ligand Adsorption and Exchange on Gold Nanoparticles. *Phys. Chem. Chem. Phys.* **2018**, *20*, 1381−1394.
(31) Skoglund, S.; Blomberg, E.; Wallinder, I. O.; Grillo, I.; Pedersen, J. S.; Bergström, L. M. A Novel Explanation for the Enhanced Colloidal Stability of Silver Nanoparticles in the Presence of an Oppositely Charged Surfactant. *Phys. Chem. Chem. Phys.* **2017**, *19*, 28037−28043.
(32) Lim, J.; Lee, N.-E.; Lee, E.; Yoon, S. Surface Modification of Citrate-Capped Gold Nanoparticles Using CTAB Micelles. *Bull. Korean Chem. Soc.* **2014**, *35*, 2567−2569.
(33) Kazakova, J.; García-Povea, A.; Fernández-Palacios, M.; Villar-Navarro, M.; Carnerero, J. M.; Jimenez-Ruiz, A.; Prado-Gotor, R. A Colorimetric Study of the Interaction of Cationicand Anionic Surfactants with Anionic Gold Nanoparticles. *Colloid Polym. Sci.* **2017**, *295*, 2141−2149.
(34) Song, J.; Huang, P.-C.; Wan, Y.-Q.; Wu, F.-Y. Colorimetric Detection of Thiocyanate Based on Anti-aggregation of Gold Nanoparticles in the Presence of Cetyltrimethyl Ammoniumbromide. *Sens Actuators, B* **2016**, *222*, 790−796.
(35) Scholl, J. A.; García-Etxarri, A.; Koh, A. L.; Dionne, J. A. Observation of Quantum Tunneling Between Two Plasmonic Nanoparticles. *Nano Lett.* **2013**, *13*, 564−569.
(36) Paredes, S.; Tribout, M.; Sepulveda, L. Enthalpies of Micellization of Quaternary Tetradecyl- and Cetyltrimethylammonium. *J. Phys. Chem. A.* **1984**, *88*, 1871−1875.
(37) Gómez-Graña, S.; Hubert, F.; Testard, F.; Guerrero-Martínez, A.; Grillo, I.; Liz-Marzán, L. M.; Spalla, O. Surfactant (Bi)Layers on Gold Nanorods. *Langmuir* **2012**, *28*, 1453−1459.
(38) Young, K. L.; Jones, M. R.; Zhang, J.; Macfarlane, R. J.; Esquivel-Sirvent, R.; Nap, R. J.; Wu, J.; Schatz, G. C.; Lee, B.; Mirkin, C. A. Assembly of Reconfigurable One-dimensional Colloidal Superlattices due to a Synergy of Fundamental Nanoscale Forces. *Proc. Natl. Acad. Sci. U.S.A.* **2012**, *109*, 2240−2245.
(39) Smith, A. M.; Johnston, K. A.; Crawford, S. E.; Marbella, L. E.; Millstone, J. E. Ligand Density Quantification on Colloidal Inorganic Nanoparticles. *Analyst* **2017**, *142*, 11−29.
(40) ten Hove, J. B.; Schijven, L. M. I.; Wang, J.; Velders, A. H. Size-controlled and Water-soluble Gold Nanoparticles Using UV-induced Ligand Exchange and Phase Transfer. *Chem. Commun.* **2018**, *54*, 13355−13358.
(41) Mehtala, J. G.; Zemlyanov, D. Y.; Max, J. P.; Kadasala, N.; Zhao, S.; Wei, A. Citrate-Stabilized Gold Nanorods. *Langmuir* **2014**, *30*, 13727−13730.
(42) Martinsson, E.; Shahjamali, M. M.; Large, N.; Zaraee, N.; Zhou, Y.; Schatz, G. C.; Mirkin, C. A.; Aili, D. Influence of Surfactant Bilayers on the Refractive Index Sensitivity and Catalytic Properties of Anisotropic Gold Nanoparticles. *Small* **2016**, *12*, 330−342.
(43) Battistini, G.; Cozzi, P. G.; Jalkanen, J.-P.; Montalti, M.; Prodi, L.; Zaccheroni, N.; Zerbetto, F. The Erratic Emission of Pyrene on Gold Nanoparticles. *ACS Nano* **2008**, *2*, 77−84.
(44) Shen, S. K.; Hu, D. D. Fluorescent Probe as Reporter on the Local Structure and Dynamics in Hydrolysis-Condensation Process of Organotrialkoxysilanes. *J. Phys. Chem. B* **2007**, *111*, 7963−7971.
(45) Açışlı, Ö.; Karaca, S.; Gürses, A. Investigation of the Alkyl Chain Lengths of Surfactants on Their Adsorption by Montmorillonite (Mt) From Aqueous Solutions. *Appl. Clay Sci.* **2017**, *142*, 90−99.
(46) Xu, J.; Zhou, L.; Liu, H.; Hu, Y. Synthesis and Self-assembly of Gold Nanoparticles Using Gemini Surfactant as a Phase Transfer Reagent and a Stabilizer. *J. Exp. Nanosci.* **2006**, *1*, 103−111.
(47) Beyazkilic, P.; Yildirim, A.; Bayindir, M. Nanoconfinement of Pyrene in Mesostructured Silica Nanoparticles for Trace Detection of TNT in the Aqueous Phase. *Nanoscale* **2014**, *6*, 15203−15209.
(48) Takahashi, H.; Niidome, Y.; Niidome, T.; Kaneko, K.; Kawasaki, H.; Yamada, S. Modification of Gold Nanorods Using Phosphatidylcholine to Reduce Cytotoxicity. *Langmuir* **2006**, *22*, 2−5.
(49) Nichols, G.; Byard, S.; Bloxham, M. J.; Botterill, J.; Dawson, N. J.; Dennis, A.; Diart, V.; North, N. C.; Sherwood, J. D. A Review of the Terms Agglomerate and Aggregate with a Recommendation for Nomenclature Used in Powder and Particle Characterization. *J. Pharm. Sci.* **2002**, *91*, 2103−2109.
(50) Bastús, N. G.; Comenge, J.; Puntes, V. Kinetically Controlled Seeded Growth Synthesis of Citrate-stabilized Gold Nanoparticles of up to 200 nm. *Langmuir* **2011**, *27*, 11098−11105.

https://dx.doi.org/10.1021/acsomega.9b03823
ACS Omega 2020, 5, 4943−4952